

1 **Snow Avalanche Frequency Estimation (SAFE): 32 years of monitoring** 2 **remote avalanche depositional zones in high mountains of Afghanistan**

3 Arnaud Caiserman^{1*}, Roy C. Sidle¹, Deo Raj Gurung²

4 ¹ Mountain Societies Research Institute – University of Central Asia, Khorog, 736000, Tajikistan

5 A. Caiserman ORCID: <https://orcid.org/0000-0003-4580-6633> ; corresponding author: arnaud.caiserman@ucentralasia.org

6 Roy C. Sidle ORCID: <https://orcid.org/0000-0002-5004-4154>

7 ² Aga Khan Agency of Habitat, Dushanbe, 734013, Tajikistan

8 *Correspondence to:* Arnaud Caiserman (arnaud.caiserman@ucentralasia.org)

9 **Abstract.** Snow avalanches are the predominant hazards in winter in high elevation mountains. They cause damage
10 to both humans and assets but cannot be accurately predicted. Here we show how remote sensing can accurately
11 inventory large avalanches depositional zones every year in a large basin using a 32-yr snow index derived from
12 Landsat satellite archives. This Snow Avalanche Frequency Estimation (SAFE) built in an open-access Google
13 Engine script maps snow hazard frequency and targets vulnerable areas in remote regions of Afghanistan, one of
14 the most data-limited areas worldwide. SAFE correctly detected of the actual depositional zones of avalanches
15 identified on Google Earth and in the field (Probability of Detection 0.77 and Positive Predictive Value 0.96). A
16 total of 810,000 large depositional zones of avalanches occurred since 1990 within an area of 28,500 km² with a
17 mean frequency of 0.88 avalanches^{km²y⁻¹}, damaging villages and blocking roads and streams. Snow avalanche
18 frequency did not significantly change with time, but a northeast shift of these hazards was evident. SAFE is the
19 first robust model that can be used worldwide and is especially capable of filling data voids on snow avalanche
20 impacts in inaccessible regions.

21 **1. Introduction**

22 Snow avalanches are among the fastest, up to 61 ms⁻¹, and therefore most dangerous natural hazards in mountain
23 areas (Louge et al., 2012). Casualties associated with avalanches are numerous; in 2021 alone, 37 fatalities occurred
24 in the US (Colorado Avalanche Information Center, 2021) and 127 in Europe (European Avalanches Warning
25 Services, 2021), but avalanche monitoring is not consistent across the globe. Most remote mountain regions and
26 communities are not systematically monitored for avalanche occurrence. Avalanche surveys amongst remote
27 villages are sparse because regions are uninhabited; however, avalanches can block connecting roads every year
28 since avalanche volumes range from hundreds to several tens of thousand cubic meters (Gubler, 1987). Where
29 weather stations exist, avalanches can be predicted based on snow depth and other weather parameters (Greene et
30 al., 2016). However, the global weather monitoring of mountainous areas is scattered and very sparse in developing
31 nations.
32

33 To support these science and government priorities in remote mountain regions, it is necessary to introduce a user-
34 friendly, open-access method that maps snow avalanches on an annual basis across wide areas where internet
35 connection and monitoring systems are not always available. As an example, half of the land surface of
36 Afghanistan is above 2000 m a.s.l. and 80% is mountainous (Asad Sarwar, 2002). Among Central Asian nations,
37 Afghanistan's population is most at risk of avalanche hazards; 22,477 inhabitants at risk compared to 5183 in
38 Tajikistan (Chabot and Kaba, 2016). Particularly, northeast Afghanistan (Badakhshan) is one of the most
39 vulnerable regions, especially from December through March (Mohanty et al., 2019). Several international
40 initiatives have been implemented in Afghanistan to forecast avalanches or assess their risks on local communities.
41 According to USAID, 30,600 buildings are at risk of avalanches in Badakhshan based on daily snow depth
42 measurements (USAID, 2021). The Aga Khan Agency for Habitat (AKAH) collects snow depth data and uses
43 models such as Alpine3D and SNOWPACK to forecast avalanche prone regions in Tajikistan, Afghanistan, and
44 Pakistan (Bair et al., 2020). Other products have been developed, such as avalanche susceptibility and exposure
45 maps (Kravtsova, 1990; Soteres et al., 2020; World Bank, 2017). Another approach is to combine topographic
46 maps and snow data via the RAMMS:AVA models (GFDRR, 2018), but these are not open access. Finally, it is
47 possible to count the number of avalanches in each district as done by the United Nations in their map *Districts*
48 *Affected by Avalanches* (OCHA-United Nations, 2012), but this is time consuming and may miss some events
49 across large areas.

50

51 Detecting the avalanches is a challenge and requires temporal as well as spatial data, especially for large areas.
52 Remote sensing technology, both air and spaceborne, can cover large areas at different times of the year. Indeed,
53 the frequent collection of satellite images over the same area enables the detection of changes in snow cover as
54 well as other hazards, such as floods and landslides. Until recently, the use of remote sensing in avalanche detection
55 was sparse due to low resolution, and the automation of such processes was even more difficult because of the
56 lack of relevant algorithms that can compute big data (Eckerstorfer et al., 2016). Other remote sensing approaches
57 for avalanche detection have used radar, Lidar, and optical data. Radar satellites, such as Sentinel-1A and B, are
58 now commonly used for detecting mass movements by assessing backscatter signal changes between two time
59 periods (before and after movement) by a co-registration of the two images. Backscatter values provide
60 information on terrain roughness and any change indicates that a mass movement or a significant erosion event
61 occurred in a given area. Vickers et al. (2016) conducted one of the first studies utilizing Sentinel-1 products to
62 detect avalanches debris by developing an unsupervised classification. This technology seems very promising for
63 avalanche detection (Eckerstorfer et al., 2017; Malnes et al., 2015; Martinez-Vazquez and Fortuny-Guasch, 2008;
64 Schaffhauser et al., 2008; Tompkin and Leinss, 2021; Yang et al., 2020). Using TerraSAR-X and Sentinel-1
65 products, Leinss et al. (2020) mapped avalanches, demonstrating the potential of radar products in snow hazard

66 detection. However, the acquisition of frequent radar images is too recent to use this technique to detect historical
67 avalanches. In addition to optical, radar or Lidar data, other studies used Digital Elevation Models (DEMs) and
68 topographic parameters to determine the influence of terrain on avalanches in Switzerland (Maggioni and Gruber,
69 2009). Other studies incorporated other parameters such as morphology and vegetation to define potential
70 avalanche zones and ran the Avalanche Flow and Run-out Algorithm to automatically detect potentially affected
71 regions by avalanches (Barbolini et al., 2011). Moreover, the combination of snow measurements (depth) and high
72 resolution DEMs have proved useful in snow hazard detection (Bühler et al., 2018a, 2022). Lidar is being used in
73 the same regard with a higher level of precision. Lidar sensors measure snow depth before and after events at
74 submeter resolutions (Prokop, 2008; Deems et al., 2013; Prokop et al., 2013; Hammond et al., 2018). However,
75 this technology remains very expensive, and the spatial coverage is limited. Therefore, Lidar data are not suitable
76 for avalanche detection at the basin scale. In addition to Optical, Radar or Lidar data, other studies used Digital
77 Elevation Models and topographic parameters to determine the terrain influence on avalanches in Switzerland
78 (Maggioni and Gruber, 2009). Some other studies added other parameters such as morphology and vegetation to
79 define potential avalanche zones and ran Avalanche Flow and Run-out Algorithm to automatically potentially
80 affected regions by avalanches (Barbolini et al., 2011). Moreover, the combination of snow measurements (depth)
81 and high resolution DEMs proved its efficiency in snow hazards detection (Bühler et al., 2018a).

82
83 Optical data are the most available data in terms of spatial and temporal resolution as well as historical archives.
84 Thus, we used optical data to detect avalanches on a long-term basis. Landsat-5, 7 and 8 products were used as
85 their resolution (30 m, 900 m²) is sufficient to detect small avalanches (Eckerstorfer et al., 2016). Most of these
86 data are available at a global scale. Optical sensors can detect areas covered or not covered by snow and this
87 approach has been used in multiple studies during the past decade. Manual approaches or indices have been used
88 in such studies. For example, Landsat-8 Panchromatic images (15 m) in combination with radar images were used
89 to detect avalanches in Norway (Eckerstorfer et al., 2014). Such combinations were also recently used in west
90 Greenland to map a large number of avalanches after an unprecedented snow event (Abermann et al., 2019). To
91 our knowledge, only one recent study automated the detection of avalanches using remote sensing products and
92 an open-access scripting approach (Smith et al., 2020). This study downloaded avalanches annually for a given
93 region of interest using available Landsat-8 images and computed NDSI for each image. NDSI differentiated so
94 called 'supraglacial debris' from snow cover, for the date of interest. However, this approach only covers high
95 elevations areas while our study aims to detect avalanches proximate to local communities at lower elevations
96 (typically valleys). Manual and visual approaches, despite the time consuming process, can also be applied to
97 detect avalanches using high resolution images (e.g., SPOT-6), mid-resolution (e.g., Sentinel-2A and B images),
98 or even Google Earth images (Singh et al., 2020; Yariyan et al., 2020; E. D. Hafner et al., 2021). Across a wide area

99 (12,500 km²) individual snow avalanches were manually digitized using high resolution SPOT-6 images (Bühler
100 et al., 2019a). Terrain parameters like slope gradient and curvature have also been added to the avalanche detection
101 process using DEMs combined with Landsat-8 images (Bühler et al., 2018b; Singh et al., 2019). Integrated criteria
102 are therefore recommended to detect avalanches. To our knowledge, no long-term avalanches mapping studies
103 using remote sensing have been conducted in the world, especially not in Afghanistan.

104

105 The general objective of this study is to map annual depositional zones of avalanche occurrence over the past 32
106 years using Landsat image archives in Badakhshan region, Afghanistan. Such long-term monitoring is the first
107 attempt globally and enables us to map the frequency of depositional zones of avalanches that impact valley
108 communities. Thus, we used optical data to detect depositional zones on a long-term basis and built an open-access
109 script in Google Engine interface: *Snow Avalanche Frequency Estimation (SAFE)*. Landsat-5, 7 and 8 products
110 were used as their resolution (30 m, i.e., minimum detectible size of 900 m²) is sufficient to detect larger avalanches
111 (Abermann et al., 2019; Eckerstorfer et al., 2014, 2016; E. D. Hafner et al., 2021; Singh et al., 2019, 2020; Smith
112 et al., 2020; Yariyan et al., 2020). Our objective is to automatically map annual depositional zones of avalanche
113 occurrence over the past 32 years using Landsat-5, 7 and 8 image archives in the Amu Panj basin of Afghanistan.
114 SAFE is applicable in any high mountains of the world, such as Tien Shen, Himalaya, Hindu Kush, Karakoram or
115 Andes, but not restricted to these, where snow avalanches deposits can be detected every year by satellite images
116 for a long time before completely melting. These outputs are of keen interest to decision makers who can use this
117 automated process to map avalanche hazard in the future. The most vulnerable areas, villages and roads, were
118 mapped for improve future planning. In addition, this research enables the monitoring of depositional zones of
119 avalanche evolution over the past 32 years. Such analyses should strengthen local community resilience to snow
120 avalanches.

121

122 **2. Materials and methods**

123 *2.1 Study area*

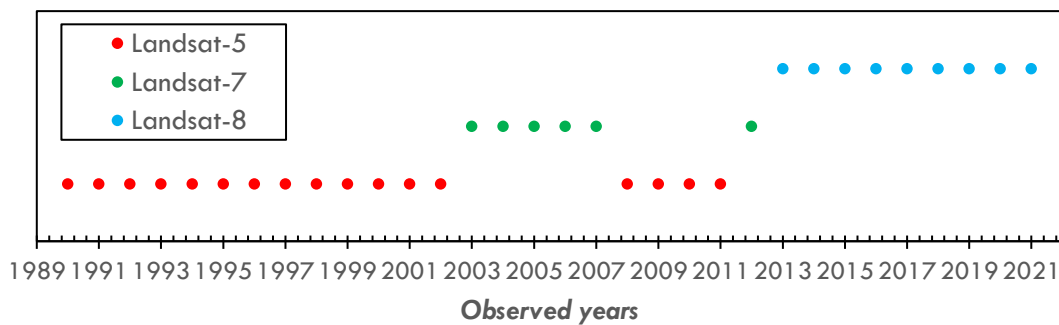
124 The study covers the most mountainous region of Afghanistan – Badakhshan in the Amu Panj basin located in the
125 northeast portion of the country. Average elevation is 2761 m and mean slope gradient is 21%. This region spans
126 from Bamyan Province to the Hindu Kush range, up through the Wakhan corridor in the far east of Afghanistan.
127 The summit is Nowshak Peak at an elevation of 7492 m a.s.l. The western part of Amu Panj basin is rather flat
128 and not prone to avalanches. Annual precipitation is about 600 mm occurring mostly as snow between February
129 and May (Zhang et al., 2015). This terrain and precipitation characteristics lend Badakhshan very prone to
130 avalanches. The basin is large (28,580 km²), justifying automated avalanche detection to cover this area in a
131 reasonable amount of time using Google Engine. Despite the remoteness of this region, Badakhshan has a

132 population of 950,953 inhabitants (Islamic Republic of Afghanistan Governmental Website, 2021) distributed in
133 4154 villages, mainly in valleys. However, 35% of the villages in Badakhshan are located at elevations above 2000
134 m, increasing the vulnerability of these communities to avalanches.

135

136 2.2 Landsat archives for snowpack analysis

137 This analysis requires the integration of numerous data into a Google Engine Java script. Firstly, a mosaic of
138 different Landsat images is created every year in the Amu Panj basin. Depending on the year of interest, Landsat-
139 5 (https://developers.google.com/earth-engine/datasets/catalog/LANDSAT_LT05_C01_T1_SR), Landsat-7
140 (https://developers.google.com/earth-engine/datasets/catalog/LANDSAT_LE07_C01_T1_SR), or Landsat-8
141 (https://developers.google.com/earth-engine/datasets/catalog/LANDSAT_LC08_C01_T1_SR) images were
142 downloaded. Within a given year the same satellite images were used. Before 1990, coverage by Landsat-5 was
143 insufficient in this region of Afghanistan. Landsat images were directly downloaded from Google Engine Archives
144 under their *ImageCollection*. Depending on the availability of images and the year of interest, one satellite or
145 another was used (Figure 1).



146

147 **Figure 1. Landsat archives used for depositional zones of avalanches detection since 1990.**

148

149 2.3 Shuttle Radar Topography Mission-30 for terrain selection

150 Detecting avalanche deposits requires terrain parameters defined by using the Shuttle Radar Topography Mission-
151 30 (<https://dwtkns.com/srtm30m/>). This Digital Elevation Model was collected in 2000 and is globally available
152 on the United States Geological Survey data portal at a spatial resolution of 30 m. SRTM-30 is used in this study
153 to delineate the regions of interest by deriving stream channels from the DEM.

154

155 2.4 Terra MODIS MOD10A2.006 for snow line analysis

156 The ROI (regions of interest) are delineated using Terra MODIS MOD10A2.006
157 (<https://nsidc.org/data/MOD10A2/versions/6>). This product of MODIS shows the snow cover (baseline: 8 days)

158 and is also globally available at a resolution of 500 m. MOD10A2.006 snow cover data are available since 2000.
159 MODIS is used to extract the seasonal snow line elevations (average) during the past 20 years in the Amu Panj
160 basin.

161

162 *2.4 Terra MODIS MOD11C3.006 for land surface temperature analysis*

163 The evolution of land surface temperature was completed using MOD11C3.006 monthly products, 0.05 degrees
164 (<https://lpdaac.usgs.gov/products/mod11c3v006/>). Temperature trends were analysed from 2000 through 2021
165 (significance > 0.05 p-value) and the slopes were extracted and plotted on monthly maps.

166

167 *2.6 Concept of the SAFE algorithm*

168 As the aim of this study is to detect and map the annual occurrence of depositional zones during the past 32 years
169 within the study area, the monitoring approach must be reasonable and transferable from year to year. Based on
170 frequent field observations and literature (Eckerstorfer et al., 2016), the authors noticed that depositional zones
171 can be detected using the contrast between snow cover and bare cover, but the timing is perhaps the most important
172 consideration. Indeed, the script is based on the assumption that snow packages exist in lowlands, especially along
173 rivers and streams, as late as May through mid-July. At this time of the year, the terrestrial snow cover has largely
174 melted and only snow packages triggered by avalanches remain. The location of those snow packages is also very
175 critical (i.e., along riverbanks). These zones are indeed detectable by delineating the depositional zones of the
176 avalanches (not their release or transition zones); in most cases these were located on river or stream banks as
177 observed in the field because the hillslopes always route snow avalanches in this direction. We cannot differentiate
178 between dry, wet, or powder snow because the process detects the remaining snow packages as avalanches in the
179 late season (spring and summer), not in winter, nor can we delineate multiple deposits within the same depositional
180 feature, only the combined deposit zones. In winter, we were not able to differentiate contrasts between snow cover
181 and avalanches, thus our focus was on the late season.

182

183 *2.7 Google Engine interface and code availability*

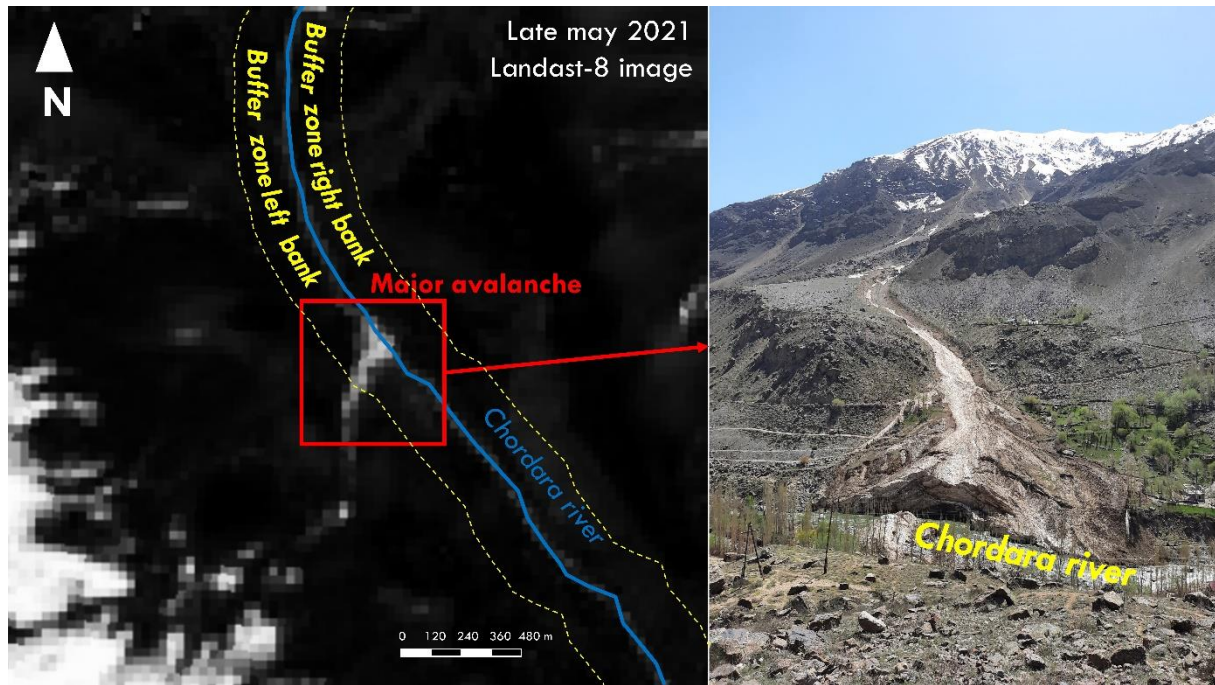
184 The concept of detecting the 'remaining snow avalanches deposits in the late season' was written in Java Script
185 using the *Google Engine* platform. The script SAFE is available at
186 <https://code.earthengine.google.com/4653677dcdc6e02d4f8dfeca2fbf670f>. We selected *Google Engine* for its
187 relative simplicity of use and open access code, which is available to all stakeholders involved in hazard and
188 vulnerability assessments. Additionally, internet connections in remote areas, such as within the Amu Panj basin,
189 are limited and powerful computers required to run scripts and process big data are sparse. Our script can be run
190 by anyone in a reasonable amount of time, even with a low internet capacity. As an example, yearly depositional

191 zones of avalanches in our study area were downloaded and mapped from Badakhshan (SAFE was processed from
192 Khorog, University of Central Asia campus, in Tajikistan) in 11.3 h (about 20 min per year of record) with an
193 average connection of 2.2 Gb/s.

194

195 2.8 Region of interest

196 The first step of SAFE is to define a region of interest as a mask to clip the Landsat images using SRTM-30 and
197 MOD10A2.006. Avalanche deposits that terminated on riverbanks, rivers, and streams are derived from SRTM-
198 30 DEMs using *ArcHydroTool* in *ArcGIS Pro Software*. Buffers of 200 m on both sides of rivers and streams are
199 defined to: (1) catch the depositional zone of avalanches that terminate in rivers and (2) increase the probability of
200 excluding the snow coverage in higher elevations that may remain throughout the summer. As an illustration, a
201 major avalanche occurred in the border zone of Afghanistan and Tajikistan in winter 2021. The remaining
202 depositional zone was still distinct in late May and June of that year on the bank of Chordara River (Figure 2).
203



204

205 **Figure 2. An illustration of avalanche depositional zone detection using late snow season Landsat-8 image**
206 **near Khorog in May 2021 (Badakhshan in Tajikistan)**

207 2.9 Date range of interest

208 A 200 m riparian buffer was used as a mask to clip the Landsat images. Because our area of coverage encompasses
209 very different elevations, the date of snow melt is not uniform throughout the basin. Therefore, distinguishing

210 between the depositional zone and bare land requires different times depending on elevation. To accomplish this,
 211 we calculated the average elevation of the snowline for the last 20 years using MODIS products. To distinguish
 212 the different melt timing between highlands from lower areas, we selected the summer snowline (June-July-
 213 August; JJA). The average elevation of the JJA snowline was 4420 m during the past 20 years. Two masks were
 214 therefore produced: one with a river buffer in lowlands and another for highlands. Those masks are only relevant
 215 if the user carefully selects the date of interest. For lowlands (below 4420 m), our time window was 15 May to 15
 216 June, indicating that the script downloads and compiles all available Landsat images acquired in this range and
 217 detects the deposit zones efficiently because during that period the terrestrial snow cover has already melted and
 218 the deposits are easily recognised. For higher elevations (above 4420 m), snow cover melted later; dates to
 219 accurately distinguish the remaining snow packages ranged from 15 June to 15 July. After many tests, it was
 220 confirmed that these date ranges reproduced the desired snow conditions during the entire 32-y period. In the
 221 script, users can modify these dates (line 24 and 112) to conform to local conditions.

222

223 *2.10 Snow index reclassification*

224 After the construction of the mask, SAFE proceeds as outlined in Figure 3. NDSI is selected to detect snow of
 225 deposit zones in the script for its transferability from one Landsat generation to another. NDSI computes a ratio
 226 between VIS and SWIR bands of Landsat satellites with negative NDSI representing non-snow cover and positive
 227 values indicating snow coverage (Equation 1). Three cover types were distinguished to detect depositional zones
 228 of avalanches at the correct time: (1) bare lands; (2) water bodies; and (3) snow. The values in Table 1 were
 229 established after multiple tests before obtaining sufficient precision to distinguish deposit zones from other land
 230 covers. On each mosaic (composite of the available images during the period of interest), a cloud mask is applied
 231 using Landsat QA bands in the script to remove clouds from the scene.

232

$$\frac{\text{Band 4} - \text{Band 6}}{\text{Band 4} + \text{Band 6}} \quad \text{Equation 1}$$

233

234 **Table 1. NDSI discrete values for avalanche depositional zones detection**

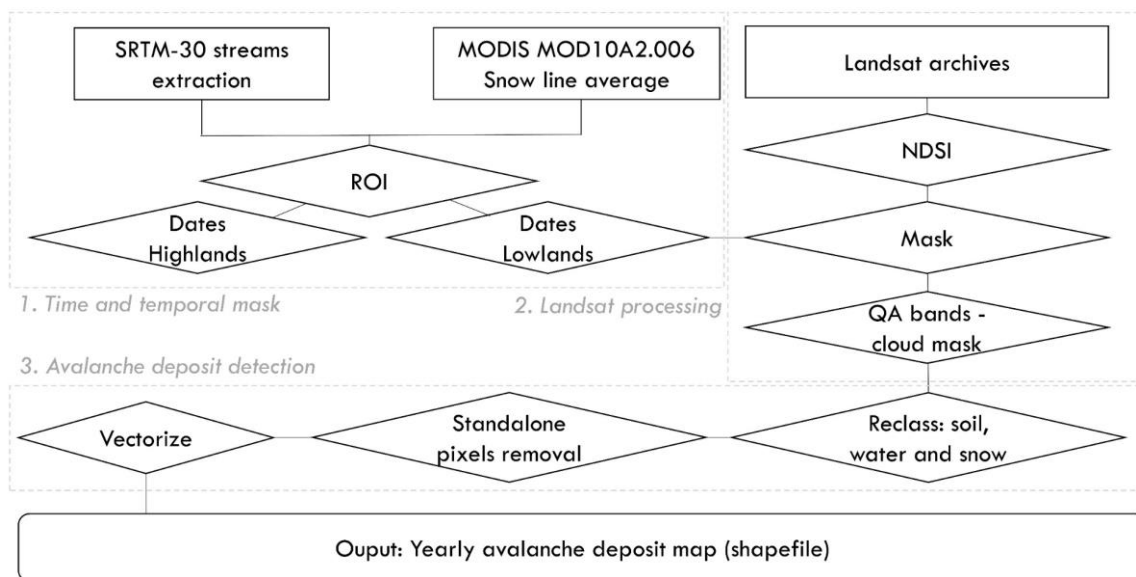
<u>Coverage</u>	<u>NDSI values</u>
Bare soil	-1 to -0.05
Water bodies	-0.051 to 0.30
Snow cover	0.31 to 1

235

236 *2.11 Depositional zone selection*

237 This further step reclassifies annual NDSI layers using ranges of values in Table 1. Only ‘snow cover’ that
 238 designates snow avalanche deposit zones is selected in the script. From the selected reclassification, the script

239 removes the standalone pixels because their classification might not be precise or representative of actual cover.
 240 Next, the selected ‘avalanche pixels’ are verified into the script avoiding manual vectorization after the
 241 downloading process. The vectorization procedure of depositional zones of avalanches is justified by the analysis
 242 steps and post-processing after downloading data. Depositional zones of avalanche statistics, elevations, and
 243 surface areas are extracted from vector files. Finally, annual avalanche deposit zone shapefiles are exported into
 244 the Google Drive user’s account.



245
 246 **Figure 3. Flow chart for Snow Avalanche Frequency Estimation (SAFE) using Landsat archives in Google**
 247 **Engine.**
 248

249 *2.12 Depositional zones of avalanche surface area classification*

250 Once the data are downloaded and imported into the GIS environment, statistical analysis commences. Every year,
 251 the number and areas of deposit zones are calculated to quantify their evolution. Moreover, the surface areas of
 252 the depositional zones are classified. Although a generic surface area classification exists (Greene et al., 2016),
 253 we decided to classify avalanches by surface areas based on local conditions. We segregated four discrete
 254 categories of deposit zones: small (< 1000 m²); medium (1000-5000 m²), large (5000-15,000 m²), and very large
 255 (15,000-100,000 m²). Such a classification enabled us to assess the intensity and potential impact of those hazards
 256 in specific locations. SAFE is not able to detect the avalanches at their time occurrence, and since these hazards
 257 are detected weeks after initiation, their surface area is underestimated by SAFE due to melting. However, the
 258 estimated surface areas in SAFE are still useful for classifying depositional zones of avalanches by surface area

259 since large snow deposits melt slower than small snow deposits. The small avalanches that occurred in winter will
260 appear as small deposit at the time of extraction in SAFE and the large events as large hazards since visible snow
261 deposits can be seen in late spring.

262

263 **3. Results**

264 *3.1 Validation*

265 The performance of SAFE in correctly detecting snow avalanche depositional zones required careful assessment.
266 To achieve this, we collected datasets that show actual locations (Global Positioning System) of avalanches that
267 occurred in the Amu Panj basin during the last 32 years. A total of 158 snow avalanche depositional zones were
268 easily identified in the riparian buffer zones on Google Earth images in 2001, 2003, 2015, 2017, and 2019. No
269 other Google Earth images were available during the last 32 years in Afghanistan, therefore the comparison
270 between SAFE and the true events was conducted with those available 158 deposit zones. These 158 deposits were
271 extracted from Google Earth and stacked with SAFE outputs. SAFE deposits were considered as valid when the
272 two datasets were overlapped at the same location and when more than half of the polygons surface extracted from
273 SAFE was overlapping the actual deposits visible on Google Earth images. Here we used statistical measures to
274 assess the performance of SAFE through the Probability of Detection (POD; Equation 2, based on (E. D. Hafner
275 et al., 2021)):

276

$$277 \quad \text{POD} = \text{true positive deposit zones} / (\text{true positive deposit zones} + \text{false negative deposit zones})$$

278

Equation 2

279

280 where *true positive deposit zones* are the avalanches detected by SAFE that were actually visible on Google Earth
281 images (in valleys where GE images were available) and *false negative deposit zones* are the locations where SAFE
282 did not detect deposit zones that had actually happened. Moreover, Positive Predictive Value (PPV; Equation 3)
283 was calculated to assess the number of times SAFE found an actual avalanche deposit zone on the ground as
284 follows:

285

$$286 \quad \text{PPV} = \text{true positive deposit zones} / (\text{true positive deposit zones} + \text{false positive deposit zones})$$

287

Equation 3

288

289 where *false positive deposit zones* are avalanche deposits predicted by SAFE that had never occurred.

290

291 The results suggest a good reliability of SAFE (Table 2). The overall POD is 0.77 which means that SAFE
 292 identified a significant number of the depositional zones of avalanches that impacted valley bottoms. Moreover, it
 293 seems that SAFE performs better in detecting true positive deposit zones (that occurred on the ground), as shown
 294 by the high PPV scores (average: 0.96). SAFE almost never detected depositional zones of avalanches that did not
 295 exist. However, SAFE might miss some deposit zones due to cloud cover on the Landsat images, especially in
 296 2001 (Table 2; POD = 0.42 in 2001).

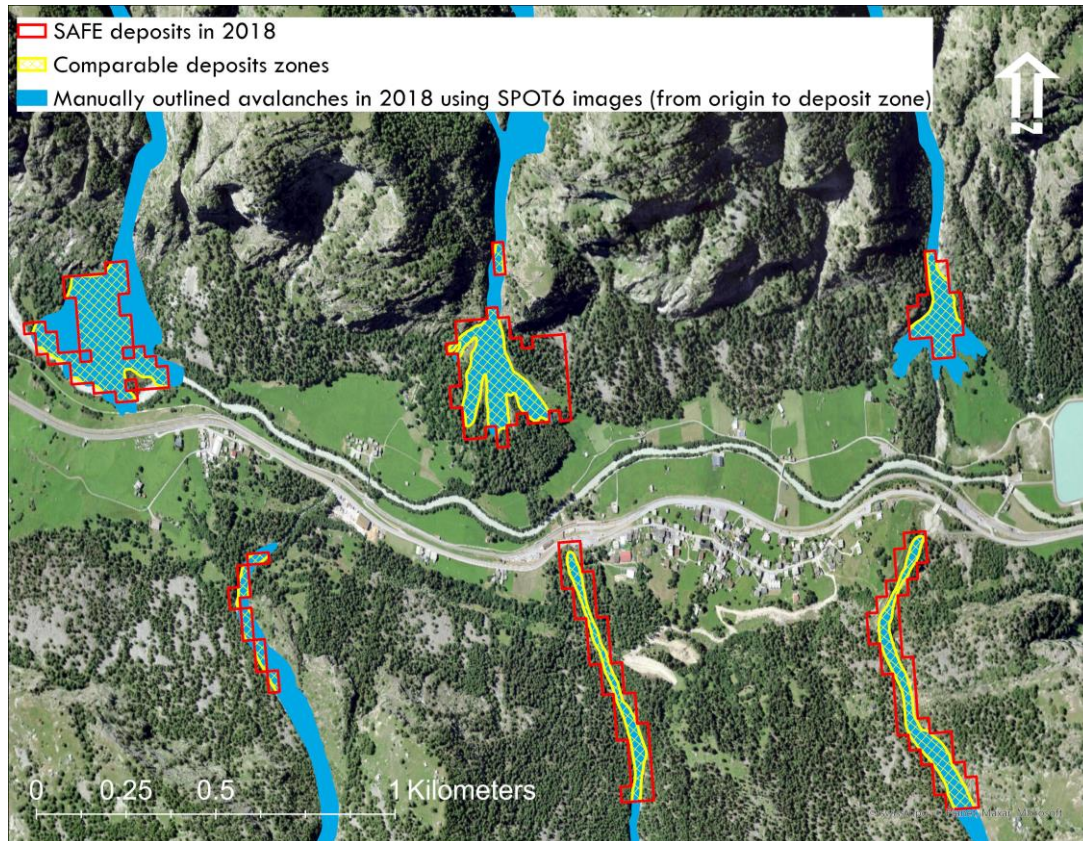
297
 298 **Table 2. Probability of detection and Positive Predictive Values of SAFE**

Statistics	2001	2003	2015	2017	2019	Average
True positive	10	35	12	19	48	
False negative	14	6	1	4	9	
False positive	1	0	0	1	3	
POD	0.42	0.85	0.92	0.83	0.84	0.77
PPV	0.91	1.00	1.00	0.95	0.94	0.96

299
 300 Another source of error arises when SAFE cannot detect depositional zones due to a dark color on the snow surface
 301 associated with surface debris or a debris flow on top of the deposit zones. NDSI may have identified those debris
 302 layers as bare soil in the classification. Moreover, it should be understood by the users that another limitation is
 303 that SAFE does not detect early winter avalanches deposits due to melting and snow coverage on and around the
 304 snow deposit, which might affect the deposits frequency estimations. However, based on our findings, SAFE can
 305 be considered as a conservative, yet robust and efficient tool to automatically identify snow avalanche depositional
 306 zones in very remote areas and can be applied in any mountainous region.

307
 308 *3.2 SAFE outputs compared with outlined avalanches using SPOT-6 images*

309 As a potential method of strengthening our testing of SAFE, outputs of our model were compared with a method
 310 that applied a more precise and expensive remote sensing product in Switzerland in 2018 (Bühler et al., 2019b;
 311 Hafner and Bühler, 2018). The Swiss area encompassed 12,500 km² where more than 18,000 snow avalanches
 312 were manually digitized using very high-resolution products SPOT-6 images (in January 2018). While our dataset
 313 is quite different from the Swiss data, the objective of this comparison was to assess how many snow avalanche
 314 deposits SAFE could detect compared to the approach using SPOT-6 (Table 3). Figure 4 shows an illustration of
 315 this comparison. It appears that the deposit zones detected by SAFE are in line with SPOT6 outlined avalanches.
 316 The later however covers the entire avalanches while SAFE only detects, automatically, the deposit zones.



317

318 **Figure 4. An illustration of the comparison between automatic detection of deposit zones using Landsat**
 319 **archives in SAFE and manually outlined snow avalanches (from origin to deposit zones) using SPOT6**
 320 **images in Switzerland**

321

322 **Table 3. Comparison of snow avalanches deposits zones between SAFE outputs (April to June 2018) and**
 323 **manual digitization using high-resolution SPOT-6 images in Switzerland in January 2018***

<u>Method</u>	<u>Number of snow polygons</u>	<u>Area of snow polygons (m²)</u>
SPOT digitization	7574	362,187,741
SAFE detection	9948	494,454,599
Overlapping SPOT-SAFE	2194	223,907,868

324

*SPOT data based on (Bühler et al., 2019b; Hafner and Bühler, 2018)

325

326 Importantly, not all avalanches manually digitized on SPOT-6 images were comparable to SAFE results. To make
 327 this comparison more consistent, we clipped the outlined avalanches with the valley bottom mask used in SAFE.
 328 Following this modification, the SPOT-6 digitization process identified 7574 avalanches deposits in valley bottoms

329 compared with 9948 by SAFE. Overlapping these two datasets, we found that both approaches detected 2194
330 deposit zones in common. Much of this discrepancy is due to the timing of SAFE images, which examine deposits
331 that remain in late spring and early summer, whereas SPOT digitization covered only January. The larger number
332 of snow deposits detected by SAFE occur during late season snow avalanches that impact valleys. This suggests
333 that SAFE could not detect all January snow deposits because many of those already melted by the time of SAFE
334 detection (early April to late June in the Swiss case). In addition, optical image quality strongly depends on cloud
335 cover that may cause avalanches to be obstructed. For instance, we could not compare the 2019 SPOT-6 derived
336 dataset in eastern Switzerland (E. Hafner et al., 2021) due to cloudy images at the end of winter and early spring
337 because these snow avalanches had already melted, implying that SAFE is more suitable for high mountain areas
338 (>4000 m) where snow deposits remain longer in valleys, thus inflicting greater damages and obstructions. Using
339 LANDSAT images, SAFE somewhat circumvents this problem of cloud cover by assessing many years of data
340 (in our case 32 y). However, SAFE does not distinguish individual events and considers overlapping snow deposits
341 as one, in contrast to SPOT-6 which distinguishes these as discrete events. This, in addition to the different methods
342 and spatial resolution difference between SAFE and SPOT, explains the somewhat low number of overlapping
343 snow deposits between SAFE and SPOT. Moreover, the SPOT digitization procedure found a total avalanche area
344 of 362,187,741 m² in January, while SAFE detected 494,454,599 m² of deposits at the end of the avalanche season,
345 including 223,907,868 m² in common. The area detected by SAFE is naturally larger than SPOT-6 since SAFE
346 maps all detectable deposits at the end of the winter. Moreover, SAFE did not detect the small avalanches of
347 January that rapidly melted after they occurred. The polygons extracted by SAFE using Landsat images are
348 obviously coarser than those outlined with SPOT-6 images, which partly explains the low number of overlapping
349 snow deposit zones, but a much more comparable detected area (62%) between the two methods. Much of the
350 discrepancy is related to SAFE's inability to detect individual events and missing deposits that rapidly melt (mostly
351 from the early winter snow avalanches), as well as the very different resolution of these products.

352

353 *3.3 Snow avalanche depositional zone frequency from 1990 to 2021*

354 By compiling 32 years of satellite images (see Methodology), the frequency of avalanche depositional zones at a
355 900 m² pixel scale was determined (Figure 5 and 6a). SAFE inventories snow avalanche deposits that occurred
356 within a year and therefore identifies the most vulnerable areas, but it does not aim to forecast future avalanches.
357 During this period, some 810,000 depositional zones impacted valleys within the Amu Panj basin (28,500 km²),
358 i.e., approximately 28 depositional zones km⁻². Each year these avalanche deposits cover an average of 1.23% of
359 the basin area but surface area varies from year to year. Avalanche depositional zone surface area ranged from 900
360 to 100,000 m² and is categorized into four classes: small (< 1000 m²); medium (1000-5000 m²), large (5000-15,000
361 m²), and very large (15,000-100,000 m²). The most frequent are medium surface area deposit zones; 342,000

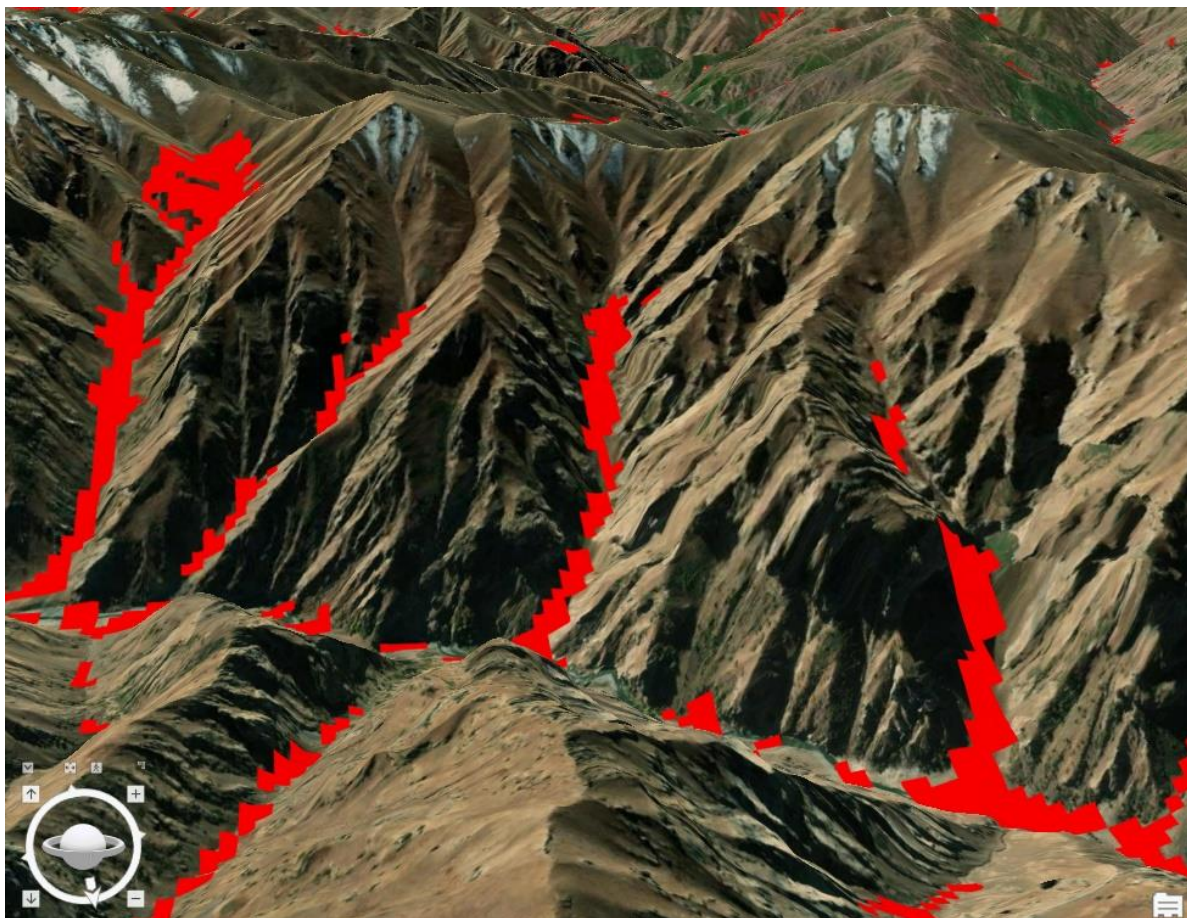
362 events during the past 32 years. Our approach also identifies very large snow avalanches depositional zones that
363 pose the greatest danger to local populations and infrastructure. We found no correlation between altitude of
364 depositional zones and their surface areas. Avalanches deposits in this region have an average altitude of 3820 m
365 and the lowest depositional zone occurred at 1755 m.

366

367 These spatial and temporal statistics allow for a geographic assessment of the avalanche deposits. In total, ten sub-
368 catchments (ranging from 18 to 240 km²) were impacted by more than one avalanche depositional zone km⁻²y⁻¹,
369 with an average frequency of 0.26 deposit zones km⁻²y⁻¹ throughout the Panj Amu basin (Figure 7). More
370 importantly, these maps prioritize villages prone to avalanches deposits and inform relevant stakeholders which
371 villages and infrastructure are most at risk. Of the 4154 villages in the region, 50 are impacted by at least one
372 avalanche within a 1 km radius each year (Figure 8). These susceptible villages are in Upper Badakhshan in the
373 north of our study area and in the Wakhan Corridor in the east where the highest mountains and most remote
374 villages are located. During the 32-y period, 92 villages were affected by very large avalanches depositional zones
375 in Badakhshan and Wakhan. Since 2019, Aga Khan Agency for Habitat (AKAH) is monitoring villages of
376 Afghanistan that have been impacted by snow avalanches. In total, 217 villages have been impacted by avalanches
377 deposit zones and those are located in the same vulnerable valleys detected by SAFE, namely High Badakhashan
378 and the Wakhan corridor.

379

380 Our remote sensing approach facilitates innovation in snow avalanche depositional zone monitoring: i.e., detecting
381 avalanches deposits outside of populated areas, especially along roads that are frequently blocked by avalanches
382 (Figure 9). More than 2000 roads in the basin (5.47% of the road network) were affected by avalanches deposits
383 every year. Additionally, more than 400 roads in Upper Badakhshan and Wakhan regions experienced more than
384 2 avalanches depositional zones y⁻¹ km⁻¹ of road (within a 1 km buffer). The average frequency along roads is 0.86
385 avalanche deposits km⁻¹y⁻¹ during the past 32 years, most of these in the medium- surface areas category.



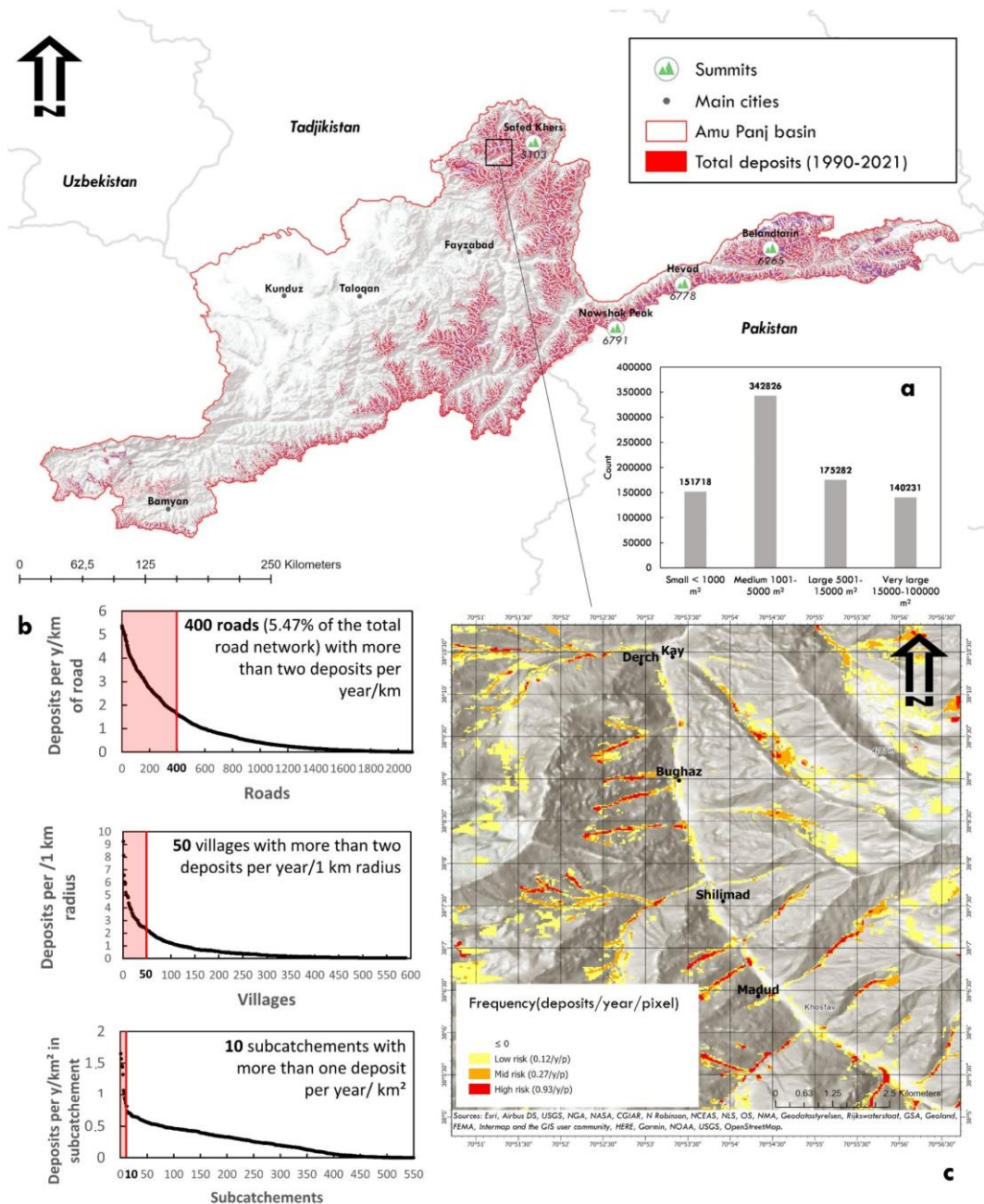
386

387

388

389

Figure 5. 3-Dimension view of the 32 years avalanche depositional zones maps in Khinj village in Afghanistan (*ArcGisPro*)



390

391

392

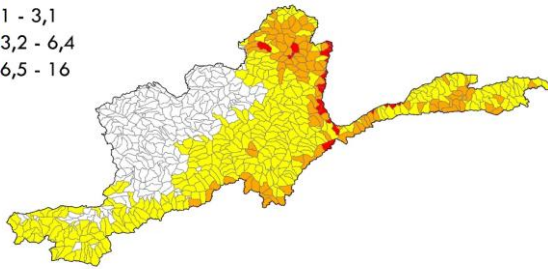
393

394

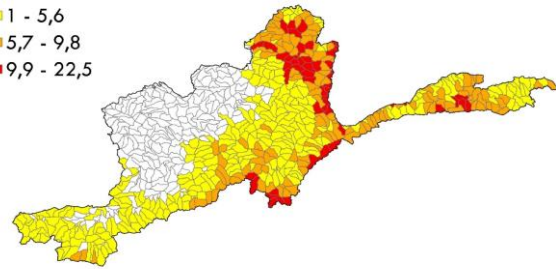
Figure 6. Yearly inventory map of snow avalanche depositional zones in the Amu Panj basin: 1990-2021: a, Surface area classification of avalanche depositional zone frequency; b, Avalanche depositional zone frequency per number of roads, villages, and subcatchments in the basin; c, An example map of avalanche depositional zone frequency during the 32-y period at a village scale.

Total snow avalanches deposits per km² in subcatchments (category 1) Total snow avalanches deposits per km² in subcatchments (category 2)

□ 0
■ 1 - 3,1
■ 3,2 - 6,4
■ 6,5 - 16



□ 0
■ 1 - 5,6
■ 5,7 - 9,8
■ 9,9 - 22,5



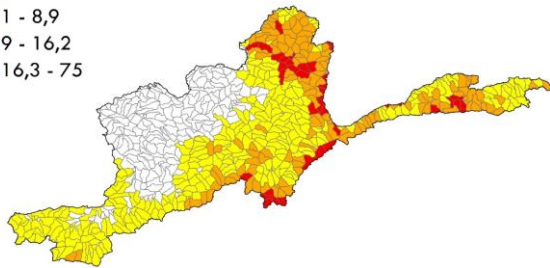
90 45 0 90 180 270 360
Kilometers



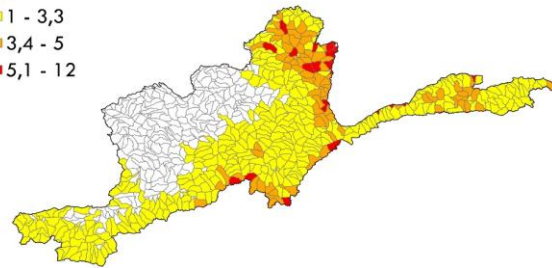
395

Total snow avalanches deposits per km² in subcatchments (category 3) Total snow avalanches deposits per km² in subcatchments (category 4)

□ 0
■ 1 - 8,9
■ 9 - 16,2
■ 16,3 - 75



□ 0
■ 1 - 3,3
■ 3,4 - 5
■ 5,1 - 12



396

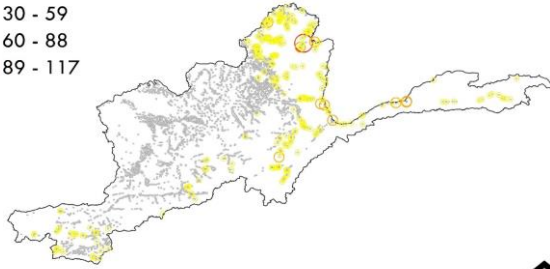
397

Figure 7. Total avalanche depositional zones per category and per square kilometer in subcatchments during the past 32 years.

398

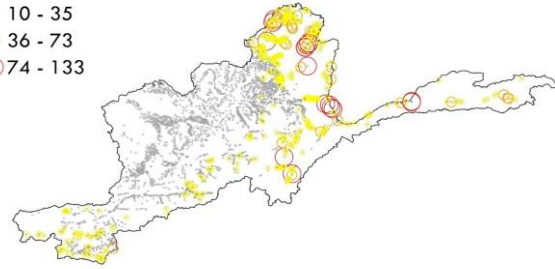
Total snow avalanches deposits per village (category 1)

- 0
- 30 - 59
- 60 - 88
- 89 - 117



Total snow avalanches deposits per village (category 2)

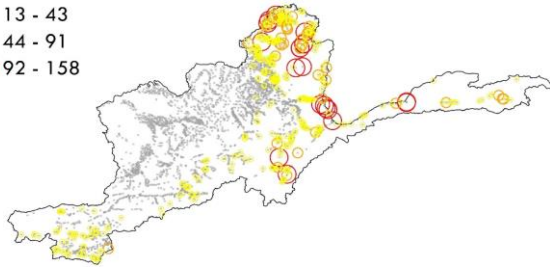
- 0
- 10 - 35
- 36 - 73
- 74 - 133



399

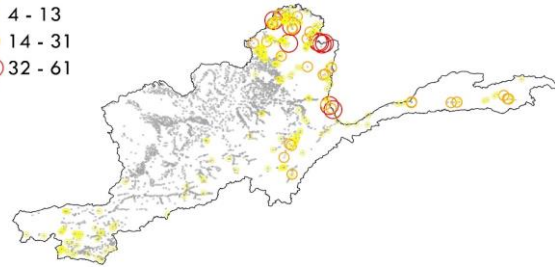
Total snow avalanches deposits per village (category 3)

- 0
- 13 - 43
- 44 - 91
- 92 - 158



Total snow avalanches deposits per village (category 4)

- 0
- 4 - 13
- 14 - 31
- 32 - 61



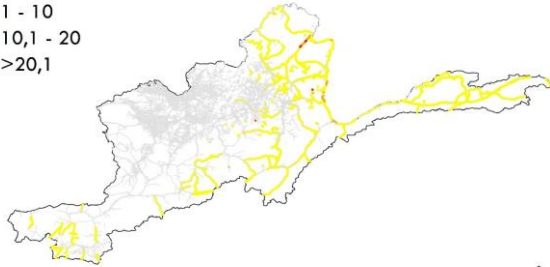
400

401

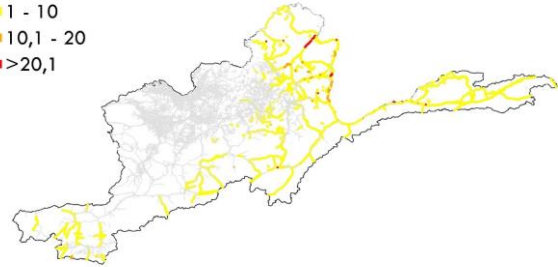
Figure 8. Total avalanche depositional zones per category and per village during the past 32 years.

Total number of avalanches deposits per kilometer of road (category 1) Total number of avalanches deposits per kilometer of road (category 2)

0
1 - 10
10,1 - 20
>20,1



0
1 - 10
10,1 - 20
>20,1



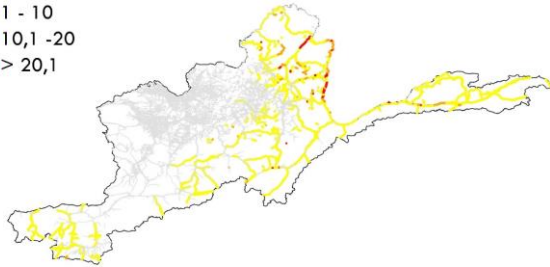
90 45 0 90 180 270 360
Kilometers



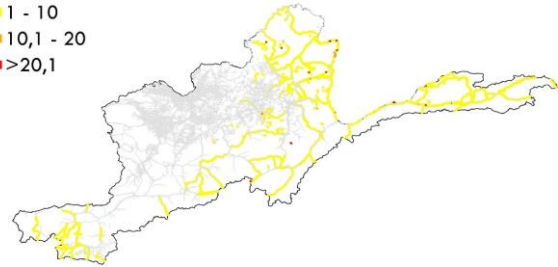
402

Total number of avalanches deposits per kilometer of road (category 3) Total number of avalanches deposits per kilometer of road (category 4)

0
1 - 10
10,1 - 20
> 20,1



0
1 - 10
10,1 - 20
>20,1



403

404

Figure 9. Total avalanche depositional zones per category and per kilometer of roads during the past 32 years

405

406

407

408

409

3.4 Stream blocking and resultant flooding

Damages to infrastructure and blocking of roads by avalanche deposits are not the only consequences of these mountain hazards. Because depositional zones typically reach rivers in this steep, incised terrain, the sudden and rapid arrival of several tons of snow can temporarily block rivers inducing short-term localized flooding. By cross-checking the map of the rivers in the Amu Panj basin with SAFE outputs, it appears that 26.2% of the river network is impacted by avalanche deposits, mainly in the high mountains. During the past 32 y, 12% of the streams have been blocked by at least 10 avalanche deposits km⁻¹ representing a significant risk for villages and farms in floodplains. The accumulated snow mass impounds river water until it can break through releasing a large discharge surge. Thus, depending on the surface area of the avalanche deposit with respect to the channel dimensions, damages to villages and farmlands may occur both upstream due to impounded water (hours to weeks) and to downstream following the sudden release of water.

3.5 Snow avalanche depositional zone trends during the past 32 years

This long-term monitoring of snow avalanche deposits facilitates the assessment of the evolution of these rapid mass movements. During the 32 years of avalanche depositional zone assessment, no significant temporal trends in impacted areas were detected (Figure 10). In addition, there was no significant trend of the surface area of snow deposits (p-value > 0.05). Nevertheless, some years posed much greater risk than others. In the last 32 years, ten years have been more at risk with above-average avalanche deposit coverage: 1990, 1991, 1992, 1993, 1994, 1995, 1996, 2003, 2005, 2007 and 2012. In particular, 2003 had many avalanche depositional zones that occupied almost 6% of the surface area of the entire basin. That year was locally noted as having heavy snowfall and farmers benefited from more snowmelt in the spring, leading to higher than average crop yields in 2003 (FAO, 2003; Guimbert, 2004). Notably, the higher risk years were also characterised by lower altitudes for avalanche deposits. There is a slight negative correlation (-0.55, Pearson test) between altitude and total annual avalanche area. With larger avalanche areas, deposits reach closer to villages. For example, in 2003, the lowest avalanche depositional zone occurred at an altitude of only 1871 m, very close to housing clusters and roads. It is therefore possible that communities below 2000 m are also impacted by snow avalanche deposits and in many mountain regions of the world this represents a significant proportion of the communities living proximate to these altitudes.

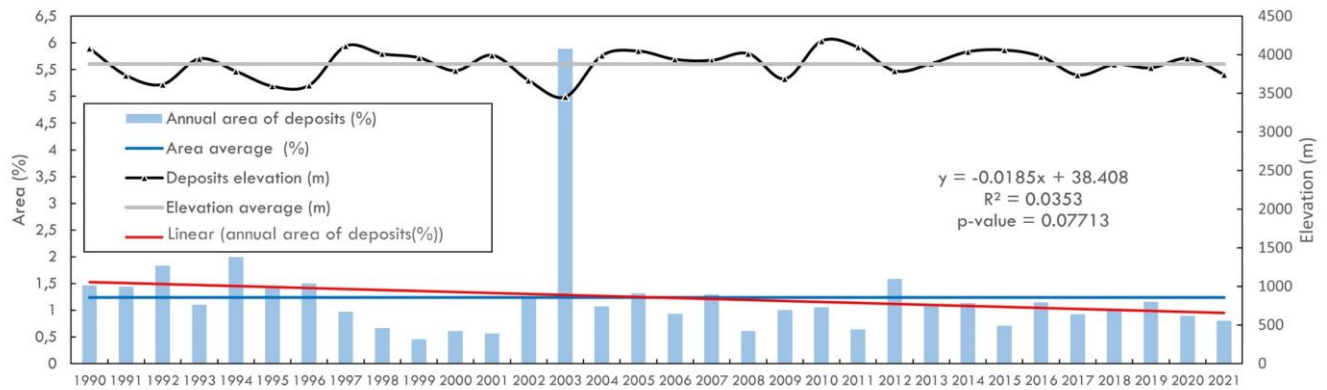


Figure 10. Snow avalanche depositional zone area and elevation trends since 1990 in the Amu Panj basin. Elevation was calculated within each polygon of avalanche deposits using SRTM-30 Digital Elevation Model. Mann-Kendall p-value 0.05 test was conducted to assess the significance of the trend.

440

3.6 Temporal geographic shifts of snow avalanches deposit zones

Long-term monitoring also shows the evolution of the spatial distribution of snow avalanche depositional zones. The pattern of snow avalanche deposits has changed with time and slightly shifted to the northeast portion of the basin; thus, more avalanches are now occurring in the northeast than in the southwest (Figure 11 a and b). Nevertheless, snow coverage did not shift simultaneously according to our remote sensing analysis nor did the snowline evolve, but rather remained variable over the last 32 years. The geographic shift of avalanche depositional zones is therefore likely due snow depth evolution. Deeper snowpacks trigger snow avalanches. There are no available data on snow depth at such a scale. However, the slope was calculated and a Mann-Kendal test was applied for each pixel of the land surface temperature images (MOD11C3). Remotely sensed land surface temperature changed during the last 20 years (Figure 11 a), with a warmer band occurring through the central portion of the basin in December (p-value 0.03 with an increase of $0.88\text{ C}^\circ\text{y}^{-1}$). This central portion is mainly mountainous and this temperature pattern may have shifted the avalanches to the northern mountains of the area, while the south is characterized by lower mountains. Overall, avalanche depositional zone locations tend to follow the spatial distribution of snow depth (Bühler et al., 2016). This means that despite the high variability of the snow line and snow coverage, the distribution of snow avalanche deposits can significantly change over time in response to temperature changes and local communities must be prepared for shifting hazards.

455

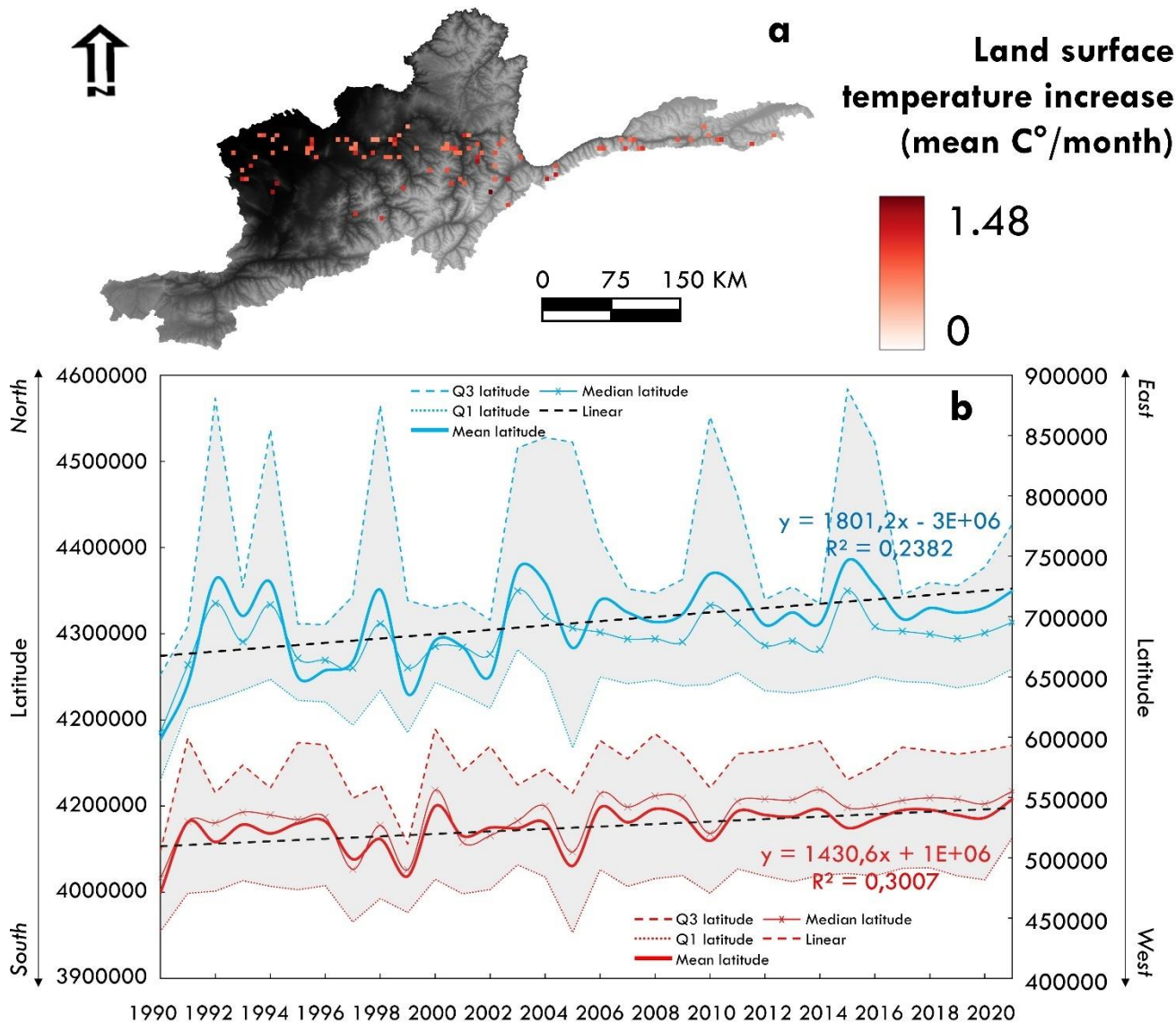


Figure 11. a, Map of areas with significant increases in monthly land surface temperatures in the Amu Panj Basin based on MOD11C3 products from 2000 to 2021; b, Geographical shift of avalanche deposits: mean longitude and latitude of avalanche deposits each year since 1990 show evidence of a movement to the northeast due to increasing winter temperature in mountainous areas.

460

4. Uncertainties and implications

4.1 Sensitivity analysis of SAFE

To better understand how SAFE works and assess its performance, a sensitivity analysis was conducted between the model parameters. The number and surface areas of avalanche depositional zones vary according to the buffer used, the dates of

465

Landsat images, and finally the NDSI range during the snow classification. The sensitivity analysis was conducted for the year 2019 when SAFE was most robust in valleys where actual avalanche deposits were quite visible on Google Earth images (POD: 0.84 and PPV: 0.94). First, we run SAFE with different buffer widths (25 m of difference between each buffer). There is a strong positive correlation (0.98) between the number of avalanche deposits detected by SAFE and the buffer width (Figure 12a). The wider the buffer around the rivers, the more avalanche deposits SAFE will detect. On the other hand, for narrower buffers, the average surface area of avalanche depositional zones is smaller (positive correlation of 0.71). This is because a large buffer extends upslope where small snow patches reside, which are not avalanche deposits since they are located at the top of hillslopes. This means that the user should not select a buffer that is too wide, rather the area should only include the riparian zone of rivers and streams where the snow avalanche deposits are located. As such, we used a value of 200 m for the entire region studied.

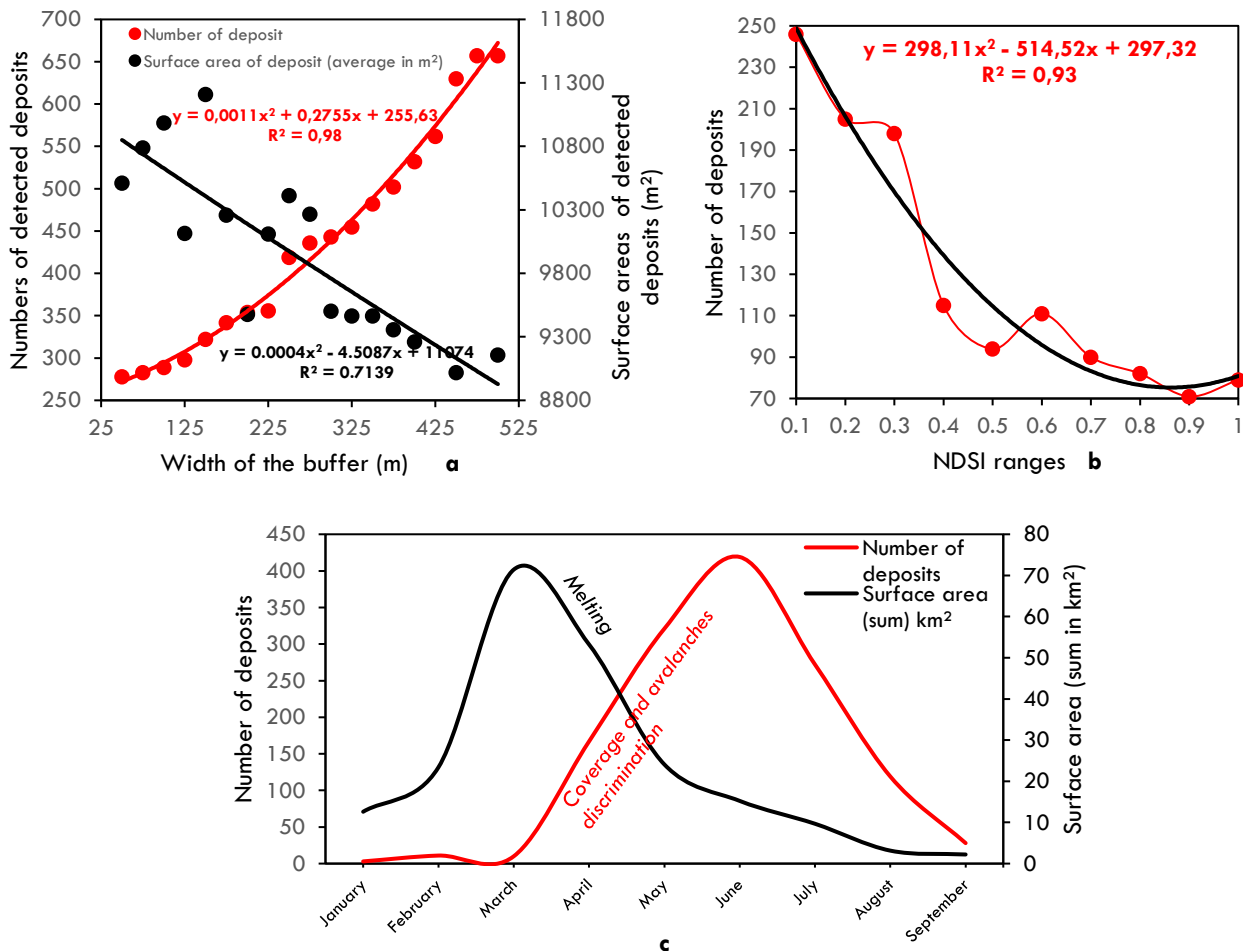


Figure 12. Sensitivity tests of SAFE for number and surface areas of detected avalanche depositional zones: a, width of buffer; b, NDSI ranges; and c, dates of interest

The number and surface areas of avalanche depositional zones detected by SAFE depends on the NDSI range when classifying snow. NDSI is used to differentiate between water bodies, bare lands, and snow. By varying the NDSI ranges of snow in the script, we notice a strong positive correlation with the number of avalanches deposits detected by SAFE. The closer the index is to 0, the more hazards SAFE finds. However, this correlation shows us that the choice of NDSI range is important because we notice a threshold at 0.31 (Figure 12b). Avalanche depositional zones seem to be more numerous with an NDSI lower than 0.31 because the snow pixels are confused with water bodies. It is therefore essential for the user to select an NDSI higher than 0.31 to distinguish water bodies (rivers, flood areas or lakes) and snow. However, there is no correlation between the NDSI ranges and the average surface areas of avalanche deposits because NDSI cannot interpret pixels other than 'snow' above the 0.31 threshold. Finally, the date of interest is a key parameter in SAFE. The number of avalanche depositional zones detected by SAFE is highest at the end of winter due to the almost constant cloud cover since January, but also due to the inability to distinguish avalanche deposits from snow cover in winter (with Landsat images) (Figure 12c). May is a key month for SAFE applications in high mountains: the snow coverage, which is thinner than the avalanche depositional zones, begins to melt and the number of avalanche deposits detected can then be assessed. It is therefore essential to select post-May images to detect avalanche deposits while taking care not to select post-July images as avalanches deposits melt in summer precluding detection.

Some avalanche deposits are also visible on successive images after the snow cover melts. SAFE was specifically designed to detect avalanche depositional zones at their earliest stage after snow melts. Indeed, starting from May (when the avalanche deposits are not confused with snow coverage), snow avalanche deposits start to melt and the surface area will begin to be underestimated. For that reason, it is important to select late spring images for lowland avalanche depositional zones and early summer for high land deposits, not later. Cloud cover is another issue in avalanche deposit locations and surface area detection since cloud cover may partly or fully obstruct the avalanche deposits at the time of the image. This is another reason to select images starting from late spring when regional cloud cover is lowest and even absent in early summer. If cloud cover is high even late spring, the users can still select later images, but there will be a risk that detected avalanche deposits will have started to melt. To summarize, we recommend the following three parameters in the SAFE script: buffer of 200 m to include only snow avalanche deposits; $NDSI > 0.31$ to distinguish water bodies from snow, and images from May to July to distinguish avalanches depositional zones from snow cover.

4.2 Excluding snow coverage

Interpreting the remaining snow packages as avalanche deposits can lead to some errors. Indeed, despite a precise masking operation (excluding summits and very high plateaus where snow persists), in some cases the use of NDSI might not properly segregate avalanche depositional zones from large areas of remaining snow. After assessing the surface area of true avalanche deposits (the ones that SAFE correctly detected based on Google Earth images), it appeared that snow cover $> 100,000 \text{ m}^2$ were not avalanche depositional zones but rather snow cover; thus, these were removed. However, in highlands, even along

515 riverbanks, some snow packages interpreted as avalanche depositional zones may be remaining snow cover. As such, the date
range for highlands was selected as late as possible in the year. Thus, it is advised to keep the mask at the very bottom of
valleys (maximum 200 m buffer along the river) to exclude high plateaus and potential snow-covered areas.

4.3 Water bodies in SAFE

520 A final limitation of using this remote sensing and NDSI approach for avalanche deposit detection is the possible confusion
between some small water bodies and avalanche depositional zones. Indeed, in some cases certain river reaches (stream order
> 4 in our study area) could be interpreted as snow because they were frozen and appeared as white pixels on Landsat archives.
The same issue can occur with ponds and lakes. This limitation was foreseen before processing the images in our study and
we excluded these large water bodies from the region of interest (in the mask) by using available shapefiles. For example,
525 Shiva Lake, one of the largest water bodies in Amu Panj basin (15 km²), was removed from the analysis. Another way to avoid
the water pixel selection is to adapt the NDSI reclassification itself, depending on the study area. This is possible in the script
lines 51-53 for low elevations and lines 139-141 for high elevations in the script.

4.4 SAFE outcomes compared to other snow avalanches detection studies

530 SAFE contributes to the literature on snow avalanche detection, but in a unique way using remote sensing. As noted, many
studies and models exist using various products: Radar, Optical, and Topographic. The strength of remote sensing is the
automatic processing at a large scale and over long timeframes. SAFE uses the capabilities of remote sensing by processing
more than one image per year at the catchment scale. Moreover, the use of Landsat archives allows assessment over the last
32 years, which is not yet possible with recent Radar data such as Sentinel-1. Most of the current avalanche detection models
535 use freely available products, with acceptable if not good accuracy (Table 4). The accuracy of these studies using Radar images
ranges from 53 to 81% making this a relatively robust tool. One of the reasons why SAFE does not use Radar images is the
weight of the images (data storage), especially Sentinel-1, which is mostly above 1 Gb/image. These heavy images are not
suitable for a model like SAFE, which was specifically designed for remote study areas where internet connections may be
very limited. Other models also exist with Optical images with high accuracy ranging from 71 to 93% (Table 4). In the optical
540 domain, SAFE showed a POD of 77% over an area of 28,500 km². SAFE is therefore in the high range of models with optical,
medium resolution (Landsat) images.

545

Table 4. References on snow avalanche accuracy using remote sensing products (Radar, Optical and Terrain)

Reference	Accuracy (%)	Dataset
Eckerstorfer et al., 2017	75	S1
Malnes et al., 2015	53*	S1
Martinez-Vazquez	76	GB-SAR LISA
Tompkin and Leinss, 2021	81	S1
Leinss et al., 2020	70	S1 and TerraSAR-X
Vickers et al., 2016	60	S1
Karas et al., 2021	70	S1
Yang et al., 2020	75**	S1
Singh et al., 2019	93	L8
Yarivan et al., 2020	90	Google Earth imagery
Hafner et al., 2021	74**	SPOT
Bühler et al., 2018	95**	DTM

550 *55 avalanches were detected using S1 image out of 102 on the field.

**POD

5. Conclusion

SAFE can be considered as a universal approach to assess snow avalanche depositional zones in spring and early summer
555 where ground data are very limited, such as in the Afghan mountains. Here we showed the capability of long-term remote
sensing data to robustly detect snow avalanche deposits that impact valley locations. While we have successively applied
SAFE to assess the frequency and impacts of avalanche deposits in valleys and lower hillslopes of Afghanistan, arguably one
of the most data-limited regions worldwide, this model should perform even better in areas where snow data are available
making it an important tool for avalanche vulnerability assessment worldwide. More than 30 years after the launch of Landsat-
560 5, it is now possible to compile all data and assess the temporal as well as spatial evolution of such hazards. NDSI is a relevant
index to detect avalanches when selecting the correct region and dates of interest - i.e., riverbanks during the late melt season.
The thickness of the depositional zones facilitates the detection of these avalanche deposits after the snow cover has melted
on hillslopes in spring or early summer. Moreover, the application of SAFE in Afghanistan, compared to its application in
Switzerland, showed that the script can be applied worldwide, especially in high mountains (above 4000 m) since deposit
565 zones are still detectable in late spring at those elevations.

The automation of snow avalanche detection using remote sensing technologies at regional scales is still new and SAFE was
designed to guide decision-makers, planners, and disaster risk practitioners. Indeed, such people can now know where the most
at-risk areas are located based on these frequency maps. Such information informs the relative risk of building sites and land
use decisions in such mountainous terrain with greater precision. The level of exposure of roads to avalanche depositional
570 zones can also be estimated using these frequency maps, and can inform road planners and managers regarding road location,

maintenance practices, and mitigation structures. Moreover, villages of high mountains such as in Afghanistan are strongly highly dependent on roads connections to provide necessary food, energy, medical supplies, and life-support items, especially in winter. It is therefore critical for local decision makers to assess the frequency of road blockage by avalanche deposits. Thus, open-access and user-friendly tools such as SAFE are highly applicable to interests of local stakeholders even with medium to
575 low power computers since SAFE uses Google servers. The tourism sector can also benefit from this snow avalanche deposit inventory, especially the winter sports industry. Furthermore, this method can also be used to prioritize areas for more sophisticated and data-intensive avalanche risk analysis (Keylock et al., 1999). SAFE can be applied by any user throughout mountainous regions of the world as it is designed to be user-friendly, and frequent users can contribute to the robustness of the snow avalanche deposit archive, thus improving recommendations for policy makers.

580

Author contributions

A.C. designed the concept of SAFE method, wrote the Google Engine script and processed the analyses of snow avalanches. A.C. and R.C.S. participated the conception of SAFE and all authors helped interpret the results. D.R.G. contributed to the writing and provided the AKAH dataset of impacted villages by snow avalanches. A.C. and R.C.S. wrote the paper.

585

Competing interests

The authors declare that they have no conflict of interest.

Acknowledgements

590 The authors are very thankful to Nusrat Nahab, Head of Emergency Management Aga Khan Agency for the Aga Khan Agency for Habitat for her support in this study and for sharing information about snow avalanches in Afghanistan. This study was implemented under the ongoing project "Addressing Climate Change in Afghanistan (E3C)" funded by the European Union, in close collaboration with Aga Khan Foundation and Wildlife Conservation Society based in Afghanistan.

References

- 595 Abermann, J., Eckerstorfer, M., Malnes, E., Hansen, B.U., 2019. A large wet snow avalanche cycle in West Greenland quantified using remote sensing and in situ observations. *Nat Hazards* 97, 517–534. <https://doi.org/10.1007/s11069-019-03655-8>
- Asad Sarwar, Q., 2002. Water resources management in Afghanistan: the issues and options. International Water Management Institute, Pakistan.
- 600 Bair, E.H., Rittger, K., Ahmad, J.A., Chabot, D., 2020. Comparison of modeled snow properties in Afghanistan, Pakistan, and Tajikistan. *The Cryosphere* 14, 331–347. <https://doi.org/10.5194/tc-14-331-2020>
- Barbolini, M., Pagliardi, M., Ferro, F., Corradeghini, P., 2011. Avalanche hazard mapping over large undocumented areas. *Nat Hazards* 56, 451–464. <https://doi.org/10.1007/s11069-009-9434-8>
- Bühler, Y., Adams, M.S., Bösch, R., Stoffel, A., 2016. Mapping snow depth in alpine terrain with unmanned aerial systems (UASs): potential and limitations. *The Cryosphere* 10, 1075–1088. <https://doi.org/10.5194/tc-10-1075-2016>
- 605

- Bühler, Y., Bebi, P., Christen, M., Margreth, S., Stoffel, L., Stoffel, A., Marty, C., Schmucki, G., Caviezel, A., Kühne, R., Wohlwend, S., Bartelt, P., 2022. Automated avalanche hazard indication mapping on a statewide scale. *Natural Hazards and Earth System Sciences* 22, 1825–1843. <https://doi.org/10.5194/nhess-22-1825-2022>
- 610 Bühler, Y., Hafner, E.D., Zweifel, B., Zesiger, M., Heisig, H., 2019a. Where are the avalanches? Rapid SPOT6 satellite data acquisition to map an extreme avalanche period over the Swiss Alps. *The Cryosphere* 13, 3225–3238. <https://doi.org/10.5194/tc-13-3225-2019>
- Bühler, Y., Hafner, E.D., Zweifel, B., Zesiger, M., Heisig, H., 2019b. Where are the avalanches? Rapid SPOT6 satellite data acquisition to map an extreme avalanche period over the Swiss Alps. *The Cryosphere* 13, 3225–3238. <https://doi.org/10.5194/tc-13-3225-2019>
- 615 Bühler, Y., von Rickenbach, D., Christen, M., Margreth, S., Stoffel, L., Stoffel, A., Kühne, R., 2018a. Linking modelled potential release areas with avalanche dynamic simulations: an automated approach for efficient avalanche hazard indication mapping. *International snow science workshop proceedings 2018* 810–814.
- Bühler, Y., von Rickenbach, D., Stoffel, A., Margreth, S., Stoffel, L., Christen, M., 2018b. Automated snow avalanche release area delineation – validation of existing algorithms and proposition of a new object-based approach for large-scale hazard indication mapping. *Natural Hazards and Earth System Sciences* 18, 3235–3251. <https://doi.org/10.5194/nhess-18-3235-2018>
- 620 Chabot, D., Kaba, A., 2016. Avalanche forecasting in the Central Asian countries of Afghanistan, Pakistan and Tajikistan. Presented at the International Snow Science Workshop, Breckenridge, Colorado.
- Colorado Avalanche Information Center, 2021. *Avalanche.org » Accidents* [WWW Document]. *Avalanche.org*. URL <https://avalanche.org/avalanche-accidents/> (accessed 6.30.21).
- 625 Deems, J.S., Painter, T.H., Finnegan, D.C., 2013. Lidar measurement of snow depth: a review. *Journal of Glaciology* 59, 467–479. <https://doi.org/10.3189/2013JoG12J154>
- Eckerstorfer, M., Bühler, Y., Frauenfelder, R., Malnes, E., 2016. Remote sensing of snow avalanches: Recent advances, potential, and limitations. *Cold Regions Science and Technology* 121, 126–140. <https://doi.org/10.1016/j.coldregions.2015.11.001>
- 630 Eckerstorfer, M., Malnes, E., Frauenfelder, R., Doomas, U., Brattli, K., 2014. Avalanche Debris Detection Using Satellite-Borne Radar and Optical Remote Sensing. *International Snow Science Workshop 2014 Proceedings, Banff, Canada* 131–138.
- Eckerstorfer, M., Malnes, E., Müller, K., 2017. A complete snow avalanche activity record from a Norwegian forecasting region using Sentinel-1 satellite-radar data. *Cold Regions Science and Technology, International Snow Science Workshop 2016 Breckenridge* 144, 39–51. <https://doi.org/10.1016/j.coldregions.2017.08.004>
- European Avalanches Warning Services, 2021. *Fatalities* [WWW Document]. *EAWS*. URL <https://www.avalanches.org/fatalities/> (accessed 6.30.21).
- 635 FAO, 2003. *FAO global information and early warning system on food and agriculture - world food programme* [WWW Document]. URL <https://www.fao.org/3/j0156e/j0156e00.htm> (accessed 10.17.21).
- 640 GFDRR, 2018. *Afghanistan Multi-Hazard Risk Assessment*. World Bank, Kabul, Afghanistan.
- Greene, E., Birkeland, K., Elder, K., McCammon, I., Staples, M., Sharaf, D., 2016. *Observation Guidelines for Avalanche Professionals in the U.S.* American Avalanche Association (No. ISBN-13: 978-0-9760118-1-1). Pagosa Springs, Victor, United States of America.
- 645 Gubler, H., 1987. Measurements and modelling of snow avalanche speeds, in: *Proceedings of the Davos Symposium*. Presented at the Avalanche Formation, Movement and Effects, Davos.
- Guimbert, S., 2004. *Structure and performance of the Afghan economy*. World, Washington D.C, United States.
- Hafner, E., Bühler, Y., 2018. *SPOT6 Avalanche outlines 24 January 2018*.
- Hafner, E., Lneiss, S., Techel, F., Bühler, Y., 2021. *Satellite avalanche mapping validation data* [WWW Document]. URL <https://www.envidat.ch/#/metadata/satellite-avalanche-mapping-validation> (accessed 3.23.22).
- 650 Hafner, E.D., Techel, F., Leinss, S., Bühler, Y., 2021. Mapping avalanches with satellites – evaluation of performance and completeness. *The Cryosphere* 15, 983–1004. <https://doi.org/10.5194/tc-15-983-2021>
- Hammond, J.C., Saavedra, F.A., Kampf, S.K., 2018. Global snow zone maps and trends in snow persistence 2001–2016. *International Journal of Climatology* 38, 4369–4383. <https://doi.org/10.1002/joc.5674>

- 655 Islamic Republic of Afghanistan Governmental Website, 2021. Badakhshan [WWW Document]. English. URL <https://president.gov.af/en/badakhshan/> (accessed 8.31.21).
- Keylock, C.J., McClung, D.M., Magnusson, M.M., 1999. Avalanche risk mapping by simulation. *Journal of Glaciology* 303–314.
- 660 Kravtsova, V.I., 1990. Snow Cover Mapping of Afghanistan’s Mountains with Space Imagery. *Mapping Sciences and Remote Sensing* 27, 295–302. <https://doi.org/10.1080/07493878.1990.10641815>
- Louge, M.Y., Turnbull, B., Carroll, C., 2012. Volume growth of a powder snow avalanche. *Annals of Glaciology* 53, 57–60. <https://doi.org/10.3189/2012AoG61A030>
- 665 Maggioni, M., Gruber, U., 2009. The influence of topographic parameters on avalanche release dimension and frequency. *Cold Regions Science and Technology, ISSW 2002: International Snow Science Workshop* 37, 407–419. [https://doi.org/10.1016/S0165-232X\(03\)00080-6](https://doi.org/10.1016/S0165-232X(03)00080-6)
- Malnes, E., Eckerstorfer, M., Vickers, H., 2015. First Sentinel-1 detections of avalanche debris. *The Cryosphere Discussions* 9, 1943–1963. <https://doi.org/10.5194/tcd-9-1943-2015>
- Martinez-Vazquez, A., Fortuny-Guasch, J., 2008. A GB-SAR Processor for Snow Avalanche Identification. *IEEE Transactions on Geoscience and Remote Sensing* 46, 3948–3956. <https://doi.org/10.1109/TGRS.2008.2001387>
- 670 Mohanty, A., Hussain, M., Mishra, M., Kattel, D.B., Pal, I., 2019. Exploring community resilience and early warning solution for flash floods, debris flow and landslides in conflict prone villages of Badakhshan, Afghanistan. *International Journal of Disaster Risk Reduction* 33, 5–15. <https://doi.org/10.1016/j.ijdrr.2018.07.012>
- OCHA-United Nations, 2012. Districts Affected by Avalanches -Badakhshan Province 19Jan.2012.
- 675 Prokop, A., 2008. Assessing the applicability of terrestrial laser scanning for spatial snow depth measurements. *Cold Regions Science and Technology, Snow avalanche formation and dynamics* 54, 155–163. <https://doi.org/10.1016/j.coldregions.2008.07.002>
- Prokop, A., Schön, P., Singer, F., Pulfer, G., Naaim, M., Thibert, E., 2013. Determining Avalanche Modelling Input Parameters Using Terrestrial Laser Scanning Technology. *International Snow Science Workshop Grenoble – Chamonix Mont-Blanc - October 07-11, 2013* 770–774.
- 680 Schaffhauser, A., Adams, M., Fromm, R., Jörg, P., Luzi, G., Noferini, L., Sailer, R., 2008. Remote sensing based retrieval of snow cover properties. *Cold Regions Science and Technology, Snow avalanche formation and dynamics* 54, 164–175. <https://doi.org/10.1016/j.coldregions.2008.07.007>
- Singh, D.K., Mishra, V.D., Gusain, H.S., Gupta, N., Singh, A.K., 2019. Geo-spatial Modeling for Automated Demarcation of Snow Avalanche Hazard Areas Using Landsat-8 Satellite Images and In Situ Data. *J Indian Soc Remote Sens* 47, 513–526. <https://doi.org/10.1007/s12524-018-00936-w>
- 685 Singh, K.K., Singh, D.K., Thakur, N.K., Dewali, S.K., Negi, H.S., Snehmani, Mishra, V.D., 2020. Detection and mapping of snow avalanche debris from Western Himalaya, India using remote sensing satellite images. *Geocarto International* 0, 1–19. <https://doi.org/10.1080/10106049.2020.1762762>
- Smith, W.D., Dunning, S.A., Brough, S., Ross, N., Telling, J., 2020. GERALDINE (Google Earth Engine supRaglAcialL Debris INput dEtector): a new tool for identifying and monitoring supraglacial landslide inputs. *Earth Surface Dynamics* 8, 1053–1065. <https://doi.org/10.5194/esurf-8-1053-2020>
- 690 Soteres, R.L., Pedraza, J., Carrasco, R.M., 2020. Snow avalanche susceptibility of the Circo de Gredos (Iberian Central System, Spain). *Journal of Maps* 16, 155–165. <https://doi.org/10.1080/17445647.2020.1717655>
- Tompkin, C., Leinss, S., 2021. Backscatter Characteristics of Snow Avalanches for Mapping With Local Resolution Weighting. *IEEE Journal of Selected Topics in Applied Earth Observations and Remote Sensing* 14, 4452–4464. <https://doi.org/10.1109/JSTARS.2021.3074418>
- 695 USAID, 2021. Afghanistan Avalanches [WWW Document]. URL <http://afghanistanavalanches.org/> (accessed 6.30.21).
- World Bank, 2017. Climate in Crisis: How Risk Information Can Build Resilience in Afghanistan [WWW Document]. URL <https://blogs.worldbank.org/endpovertyinsouthasia/climate-crisis-how-risk-information-can-build-resilience-afghanistan> (accessed 6.30.21).
- 700 Yang, J., Li, C., Li, L., Ding, J., Zhang, R., Han, T., Liu, Y., 2020. Automatic Detection of Regional Snow Avalanches with Scattering and Interference of C-band SAR Data. *Remote Sensing* 12, 2781. <https://doi.org/10.3390/rs12172781>

- 705 Yariyan, P., Avand, M., Abbaspour, R.A., Karami, M., Tiefenbacher, J.P., 2020. GIS-based spatial modeling of snow avalanches using four novel ensemble models. *Science of The Total Environment* 745, 141008. <https://doi.org/10.1016/j.scitotenv.2020.141008>
- Zhang, J., Gurung, D.R., Liu, R., Murthy, M.S.R., Su, F., 2015. Abe Berek landslide and landslide susceptibility assessment in Badakhshan Province, Afghanistan. *Landslides* 12, 597–609. <https://doi.org/10.1007/s10346-015-0558-5>